Bull Volcanol (2006) 69: 89–103
DOI 10.1007/s00445-006-0057-6

RESEARCH ARTICLE

J. E. Sable · B. F. Houghton · C. J. N. Wilson · R. J. Carey

# Complex proximal sedimentation from Plinian plumes: the example of Tarawera 1886

Received: 5 April 2005 / Accepted: 11 January 2006 / Published online: 4 April 2006


**Abstract** The 1886 eruption of Tarawera, New Zealand, was unusual for a Plinian eruption because it involved entirely basaltic magma, originated in a 17-km-long fissure, and produced extremely overthickened proximal deposits with a complex geometry. This study focuses on an 8-km-long segment cutting across Mount Tarawera where over 50 point-source vents were active during the 5.5-h eruption. A detailed characterization of the proximal deposits is developed and used to interpret the range of styles and intensities of the vents, including changes with time. We identify the four vents that contributed most heavily to the Plinian fall and evaluate the extent to which current volcanic plume models are compatible with the depositional patterns at Tarawera. Three proximal units are mapped that have phreatomagmatic, magmatic, and phreatomagmatic characteristics, respectively. Within the magmatic proximal unit, beds of like character are grouped into packages and delineated on scaled cross sections. Package dispersal is quantified by measuring the linear thickness half-distance ($t_{1/2}$) in the planes of the fissure walls. Most packages have localized dispersals (low $t_{1/2}$), indicating that Strombolian-style activity dominated most vents. The more widely dispersed packages (high $t_{1/2}$) reflect contributions from additional transport regimes that were more vigorous but still contributed considerable material to the proximal region. We conclude that the geometry of the observed proximal deposits requires three modes of fall transport: (1) fallout from the upper portions of the Plinian plumes produced principally by vents in four craters; (2) sedimentation from the margins of the lower portions of the Plinian plumes including the jets and possibly the lower convective regions; and (3) ejection by weak Strombolian-style explosions from vents that did not contribute significant volumes of particles to the high plume. We suggest that the curvature of the velocity profile across the jet region of each plume (1–4 km height) was important, and that the lower velocity at the margins allowed proximal deposition of a large volume of material with a wide grain-size range.

**Keywords** Basaltic Plinian eruption · Tarawera 1886 · Proximal Plinian fall deposit · Eruption dynamics · Jet sedimentation

Editorial responsibility J. White

J. E. Sable (✉) · B. F. Houghton · R. J. Carey
Department of Geology & Geophysics, SOEST,
University of Hawaii,
1680 East-West Road,
Honolulu, HI 96822, USA
e-mail: jesable@soest.hawaii.edu
Tel.: +1-808-9562536
Fax: +1-808-9555512

C. J. N. Wilson
Geology Department,
University of Auckland,
Private Bag 92019,
Auckland, New Zealand

## Introduction

The 1886 eruption of Tarawera volcano in the Taupo Volcanic Zone was New Zealand's largest and most destructive historical eruption (Walker et al. 1984). This event was unusual in several ways. First, although the eruption involved exclusively basaltic magma, its main phase included intense sustained activity that is rarely associated with basalt, resulting in a >10,000 $km^2$ Plinian fall deposit (Thomas 1888; Walker et al. 1984). Second, the eruptive source was a 17-km-long fissure (Fig. 1) formed by >50 vents in 13 major craters across Mt Tarawera itself as well as an uncertain number of vents to the southwest at Rotomahana (Nairn 1979; Nairn and Cole 1981; Houghton et al. 2004a). Third, in addition to the Plinian sheet of scoria fall, the eruption produced strongly over-thickened proximal deposits on Mt Tarawera that form a series of half-cones on both sides of the fissure, visible in excellent exposures at sites extremely close (90–300 m) to vent (Houghton and Wilson 1998). The geometry of the 1886 proximal deposits is extremely complex and has consequent implications for the diversity of transport and deposition processes not only for the Tarawera eruption

itself but also for Plinian plumes in general. Tarawera 1886 provides a valuable opportunity to study links between fall deposition close to vent and deposition in the far field.

## Sedimentation from Plinian plumes

Well-established models divide Plinian plumes into three regions: momentum-driven jet, convective buoyant plume, and umbrella cloud (Sparks et al. 1997 and references therein). Deposition from the umbrella cloud is well-constrained; gravity current and advection/diffusion models provide good fits with field observations of medial-distal deposits (e.g. Carey and Sparks 1986; Bursik et al. 1992; Sparks et al. 1992; Koyaguchi 1994; Bonadonna et al. 1998; Bonadonna and Phillips 2003). Less is understood about sedimentation from the jet and lower convective plume, and few have attempted to model it (Sparks et al. 1997). Bursik et al. (1992) and Ernst et al. (1996) proposed models of sedimentation from turbulent eddies at the margins of the jet and convective plume regions of the column, but the models predict that all particles smaller than a certain threshold (depending on column height) are re-entrained, resulting in near-vent deposits that are both limited in volume and coarse in grain size. We seek a model or combination of models that can account for additional complexities that we observe in the Tarawera 1886 deposits.

## The Tarawera 1886 eruption: chronology and previous studies

The sequence of events in the eruption is detailed in eyewitness accounts (summarized in Keam 1988). Key aspects are described here to provide a context for our study. On June 10, 1886, at 12:30 a.m., earthquakes were felt over a wide area, and this seismicity intensified until eruption began about 1 hour later. Shortly after 2:00 a.m., ash columns were observed above two pre-existing lava domes on Mt Tarawera, identified by eyewitnesses as

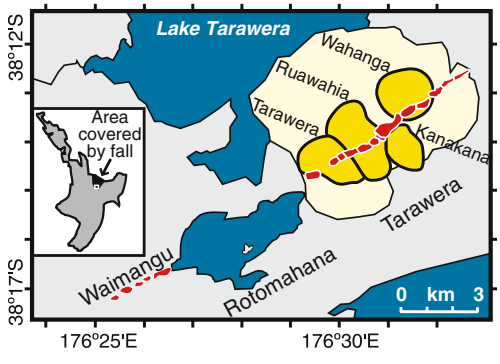


**Fig. 1** Location map with pre-1886 rhyolitic dome complex of Mt Tarawera outlined. The four main Kaharoa domes are labeled and the surrounding pre-Kaharoa lavas are a *paler shade*. Inset map shows the on-land distribution of the 1886 scoria fall in *black*, with *white rectangle* marking area of Tarawera map

Wahanga and Ruawahia domes (Fig. 1; Williams 1887). Activity spread both northeast and southwest to form an 8-km-long chain of 13 elongate craters separated by septae where the dikes did not break the surface (Nairn and Cole 1981; Walker et al. 1984). Sustained eruption produced a curtain of fountains and a plume described as more than 10 km high (Keam 1988). At 2:30 a.m. a second plume rose from a vent farther to the southwest, widely assumed to be due to initial explosions at Rotomahana (Fig. 1), a field of hot springs and fumaroles underlain by the same geothermal system that feeds the modern Waimangu field (e.g. Nairn 1979). At 3:20 a.m. a severe earthquake occurred, probably marking the time when the active geothermal system at Rotomahana began to be disrupted violently by interaction between magma and superheated water (Houghton and Wilson 1998). Activity then continued along the entire 17-km length of the eruption fissure until 6:00 a.m. (Williams 1887). In contrast with eruptions at Mt Tarawera, the explosions at Rotomahana generated both a high liquid-water-rich plume and turbulent pyroclastic density currents composed of blocks, ash, and steam, which destroyed four villages (Nairn 1979). Accumulation of fine damp ash on rooftops caused building collapses that accounted for most of the 108 known deaths (Keam 1988).

Investigation of the events began immediately after the eruption and yielded a series of published reports (Smith 1886a,b; Hutton 1887; Williams 1887; Thomas 1888). These workers recognized and mapped the widespread products of the eruption and documented the basic features that distinguish the deposits of the northeastern portion of the fissure (Mt Tarawera) from those of the southwestern portion (Rotomahana-Waimangu). Thomas's (1888) map of the 1886 deposits is one of the first isopach maps ever published.

The modern phase of investigations at Tarawera began with detailed mapping by Cole (1970). Nairn (1979) studied the southwestern deposits, focusing on the dynamics of the pyroclastic density current phases. Nairn and Cole (1981) determined that the northeastern portion of the rift is divided into a series of right-stepping en echelon segments, each containing several source vents. Walker et al. (1984) produced the most comprehensive study to date, re-mapping the distal eruption products, subdividing the proximal stratigraphy into 5 units, and proposing that the widespread scoria fall was deposited in a late stage of exceptionally vigorous activity. Keam (1988) compiled and re-evaluated all relevant historical accounts to build a more accurate record of the chronology and social effects of the eruption.

This paper is part of a larger study that focuses on the northeastern part of the 1886 fissure because it hosted the Plinian activity (Walker et al. 1984). The first two publications of this study (Houghton and Wilson 1998; Houghton et al. 2004a) re-interpreted the stratigraphy of and proposed a revised nomenclature for the proximal units, which we adopt in this paper (Table 1). The new unit 1 is the same as that of Walker et al. (1984), the new unit 2/3 is their units 2 and 3 combined, and the new unit 4/5 is

their units 4 and 5 combined. Houghton and Wilson (1998) correlated the widespread fall deposits with all of proximal unit 2/3 and proposed that intense activity was sustained for most of the eruption's duration, rather than being restricted to a late stage as in Walker et al.'s (1984) model. The third paper in the current study presents new grain size and componentry data for the three proximal units (Carey et al. in review).

## Distribution and characteristics of the 1886 deposits

The southwestern portion (Rotomahana-Waimangu) of the 1886 eruptive fissure (Fig. 1) was the source for the fine-ash-rich deposits with common accretionary lapilli collectively called the Rotomahana Mud (Nairn 1979). The southwestern deposits include localized pyroclastic density current deposits and a widespread fine-ash fall with a northerly dispersal that forms a significant component within the upper levels of the otherwise scoria-dominated 1886 fall deposits.

The northeastern portion of the fissure, which cuts the pre-existing rhyolitic dome complex of Mt Tarawera (Fig. 1), differs from the southwestern portion in the nature of its activity and resulting deposits (Walker et al. 1984; Houghton and Wilson 1998). The northeastern vents produced both sheet-forming and cone-building deposits of basaltic scoriaceous lapilli (Walker et al. 1984). The widespread scoria sheet covers an area of 6,000 km$^2$ within the 2.5 cm isopach, and an estimated total area of 10,000 km$^2$, with a dispersal axis toward the northeast (Thomas 1888; Walker et al. 1984). The large extent and low rate of thinning ($b_t$=4.3 km after Pyle 1989) qualify the deposit as Plinian, with an estimated column height of ~28 km (Walker et al. 1984). Median grain size of the widespread scoria fall decreases systematically with increasing distance, changing from −3.3 ϕ (1 cm) at 1 km to 2.3 ϕ (0.2 mm) at 40 km from vent; however, these values include up to 15% of the fine-grained Rotomahana Mud (Walker et al. 1984).

The cone-forming proximal deposits surround the 8-km-long Mt Tarawera portion of the rift and are confined to an area within 400 m of it. Complete sequences are well exposed along sub-vertical walls on both sides of the fissure. The proximal deposits are dominated by scoriaceous, phenocryst-poor, moderately to highly vesicular juvenile basalt (Walker et al. 1984). The minor wall rock component comprises fragments of rhyolitic lava and pyroclasts derived from shallow portions of the pre-existing dome complex. A distinctive feature in nearly all the basaltic pyroclasts is the presence of mm-sized rhyolite inclusions in abundances ranging from 1.1 to 3.6 wt% (Carey 2002).

Table 1 summarizes characteristics of the proximal units. Unit 1 was produced during the relatively brief phreatomagmatic initial stage of the eruption and is rich in vesicular basalt clasts and rhyolitic wall rock fragments, the former occasionally with denser outer rims indicative of rapid quenching (Houghton and Wilson 1998). Unit 2/3, correlated with the widespread Plinian fall (Houghton and Wilson 1998), is a moderately bedded red-black scoria fall deposit with alternating welded and non-welded subunits that thicken and thin along the fissure walls. At the top of the succession, unit 4/5 consists of rhyolitic wall-rock particles ranging from ash to blocks and subordinate dense juvenile basalt clasts, together with sparse Rotomahana Mud material. This unit is inferred to represent the closing phreatomagmatic to phreatic phase of the eruption (Walker et al. 1984; Houghton and Wilson 1998). Grain size data for each proximal unit are shown in Table 1.

## Questions and objectives

A number of key issues about the 1886 eruption remain unresolved, particularly about the dynamics of explosions along the northeastern, or Mt Tarawera, portion of the eruption fissure. The questions addressed in this paper include: (1) What was the range of styles and intensities present at different vents and different times? (2) Which of the >50 vents along the fissure contributed to the Plinian umbrella cloud(s)? (3) What plume model(s) can predict the variety of dispersals observed at Tarawera? Answers are sought through a detailed quantitative study of proximal deposit geometry. The results are compared with data from other deposits in order to infer a

**Table 1** General characteristics of the northeastern 1886 Tarawera deposits and comparison with the widespread fall deposits observed at medial-distal localities

| Unit | Juvenile clast morphology | Juvenile clast vesicularity | Wall rock content | Median grain size, ϕ | Sorting, σϕ | Interpretation |
|---|---|---|---|---|---|---|
| Medial-distal | Ragged, blocky | Moderate–high | Moderate | −3.3 to +2.3 | | Plinian fall |
| Proximal 1 | Ragged, breadcrusted | Moderate–high | Moderate | −4.2 to −1.4 | 2.2 to 3.4 | Initial phreatomagmatic |
| Proximal 2/3 | Fluidal, ragged, blocky | Moderate–high | Low-moderate | −6.1 to −1.8 | 1.6 to 3.2 | Main phase including Plinian |
| Proximal 4/5 | Blocky, angular | Low | High | −3.4 to −1.1 | 1.2 to 2.1 | Late-stage phreatomagmatic |

Juvenile clasts were divided into five categories: fluidal, ragged, blocky, breadcrusted, and angular, and ranked in order of abundance for each unit. Grain size and sorting data are from Carey et al. (in review)

combination of transport mechanisms that best explains the observed range of styles and dispersals. This information ultimately will permit more realistic modelling of Plinian transport and deposition in the proximal environment.

## Methods

Measurements of proximal deposit thicknesses come from 31 detailed stratigraphic sections as well as spot measurements at several locations obtained by lowering a tape measure vertically from the top of the fissure wall. The data were marked on color panoramas made from mosaics of ground-based photographs of the rift walls. The scaled photographs could then be used to interpolate thicknesses at points between measurement locations. Lateral distances were measured on the map or estimated from the scaled photographs. Isopachs were then drawn and closed using an assumption of symmetry around known vent locations. Some walls in craters A, B, C, G, and L were too inaccessible to be photographed or measured, so the data presented here are not continuous for the entire Mt Tarawera fissure.

### Study of proximal packages

In a complex setting with multiple vents, isopach maps alone are insufficient to indicate the intensity of eruptions from the individual vents. To constrain the behavior of individual vents, we divide and describe the proximal deposits on a detailed scale. Our quantitative studies focus on unit 2/3 because it formed during the Plinian phase of the eruption (Houghton and Wilson 1998).

The excellent exposures on the walls of the eruption fissure allow individual components of unit 2/3 to be delineated in the planes of the fissure walls (Fig. 3). For convenience of description, we define "packages" as groups of beds within a unit that share common characteristics of dispersal, grain size, componentry, and degree of welding. Packages were identified and mapped onto scaled photographic panoramas to create fifteen cross-sectional diagrams, eight of which are shown in Fig. 3. Each package is labeled with the letter of the inferred crater of origin and a number. Packages on the southeastern walls are distinguished by a prime mark after the letter. Numbers are not meant to represent stratigraphic order or relative age and packages with the same number on opposite sides of a crater are not correlated. For example, H5 and H′5, on the northwest and southeast sides of crater H, respectively (Fig. 3f,g), were not necessarily deposited at the same time, nor were they necessarily derived from the same vent within crater H.

A useful parameter for describing and comparing deposit dispersals is the thickness half-distance ($b_t$, Pyle 1989), the radial distance over which a deposit's thickness changes by a factor of two. Although thickness half-distance is typically calculated from isopach areas to reduce distortion due to asymmetric dispersal, the limited exposure perpendicular to the Tarawera 1886 fissure precludes estimation of isopach areas for individual packages. Instead, we measure *linear* thickness half-distance ($t_{1/2}$, Houghton et al.

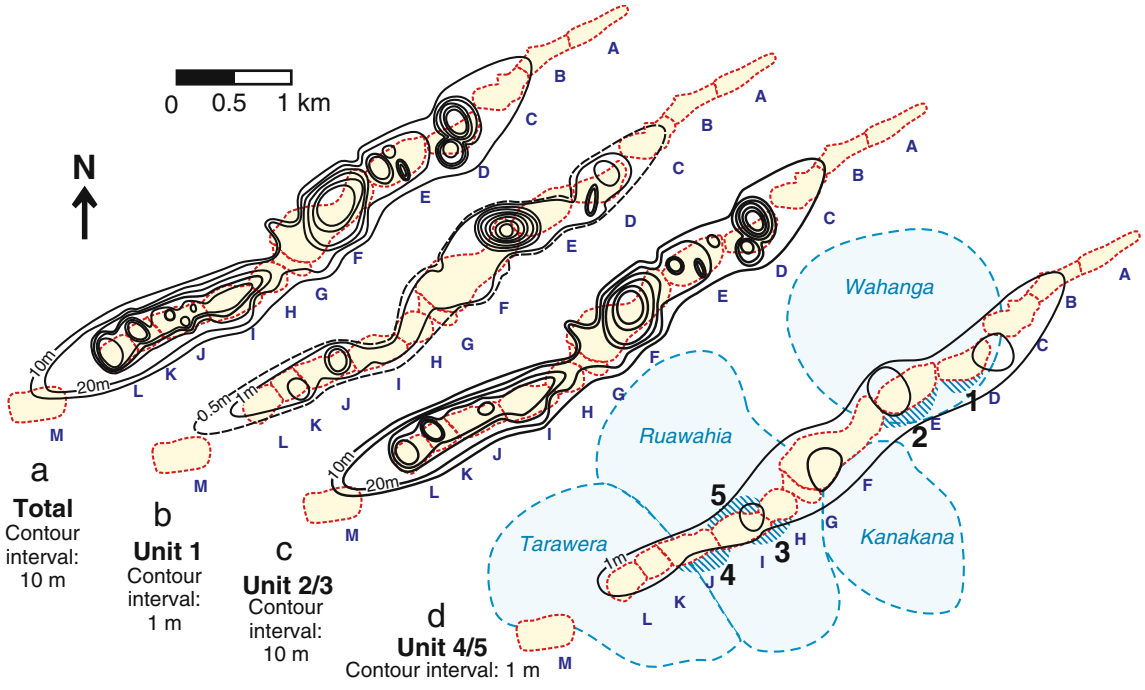


**Fig. 2** Proximal isopach maps for **a** total deposit, **b** unit 1, **c** unit 2/3, and **d** unit 4/5. Pale yellow indicates 1886 craters (*fine dotted outlines*). Contour intervals are indicated for each map. Craters are labeled with letters *A–M*. Kaharoa domes are marked with dashed outlines (**d**), and block aprons are *shaded* and numbered *1–5*

2004b) in the planes of the crater walls. The $t_{1/2}$ values may be directly compared with $b_t$ values (Pyle 1989) from other deposits if it is assumed that the 1886 packages are radially symmetric. Even if the packages are not perfectly symmetric due to wind or varying ejection angles, the $t_{1/2}$ values are still useful for comparisons among Tarawera packages.

## Results

### Thickness trends of proximal units

First, bulk properties of the proximal deposits are described for the whole Mt Tarawera fissure. Figure 2 shows isopach diagrams for the entire proximal deposit and for units 1, 2/3, and 4/5 individually. The total proximal deposit (Fig. 2a) is at least 10 and more typically >20 m thick almost everywhere along the fissure's edges, but thins rapidly away from the rift, decreasing to <10 m within 600 m of most of the inferred vent locations. Total thicknesses on the fissure walls range from 15 to 70 m and vary on an extremely local scale, such that thicknesses may change from 20 to 60 m within single crater segments over distances of tens to hundreds of meters (e.g. craters D, F, L; Fig. 2a). Thicknesses of individual units vary independently. For example, unit 1 is thickest at locations in craters D, J, and the northeastern corner of F (Fig. 2b), while the thickness maxima for unit 2/3 are in craters D, F, K, and L (Fig. 2c). Thickness patterns are asymmetric across the fissure for all proximal units.

The thickness of unit 1 (Fig. 2b) ranges from 0.5 to 8 m along the fissure's edge, but at most locations its thickness is <2 m. Unit 1 is especially thick at locations in craters D, E, F, J, and K. In particular, at the northeastern edge of crater F, unit 1 thickens from 1 to 9 m over a lateral distance of only 200 m. At this location, the contact between units 1 and 2/3 is clearly diachronous, suggesting that the influence of external water persisted longer at some sites than at others.

Unit 2/3 (Fig. 2c) ranges from <10 to 62 m thick along the fissure. The depositional pattern of unit 2/3 is more complex than those for units 1 or 4/5, with sharp changes in thickness observed between craters and even within some of the larger craters. For example, extremely localized accumulation characterizes the deposits in the northeastern end of crater D, where unit 2/3 thickens from 20 to 65 m over a lateral distance of 100 m. The other extreme is seen in craters H–J, where the thickness of unit 2/3 is uniformly 40–50 m over a distance of 700–800 m along the rift. The dramatic variations in total thickness of the 1886 products are largely controlled by the thickness of unit 2/3, which makes up 90–95% of the total 1886 deposit at most sites.

Unit 4/5 (Fig. 2d) is 1–2 m thick along most of the fissure, with minor anomalies in craters D, E, F, and I. The unit also includes several aprons of discrete 0.3–1.0-m-diameter lithic blocks that extend ≤1 km outward from some craters (labeled 1–5 on Fig. 2d). The variably thick unit 4/5 is interpreted as the product of numerous relatively weak phreatomagmatic explosions during late-stage withdrawal of magma from the fissure.

### Observations of proximal packages

No fine ash partings or erosional breaks are observed in the unit 2/3 deposits. Visible bedding within packages is formed by abrupt shifts in grain size and wall rock content or by contrasting welding states. Bedding planes dip mostly outward at moderate to steep angles. The deposits commonly mantle the pre-1886 topography, but in some places thicken to fill valleys (e.g. D1 and H7 in Fig. 3b,f). The upper and lower boundaries of packages are distinct over most of the length of each crater, but the lateral terminations of packages are not. Horizontally adjacent packages merge end-to-end with no clear boundary, indicating that neighboring vents erupted simultaneously with overlapping dispersals.

The majority of packages are confined within single craters, suggesting that most of the ejecta fell within tens to hundreds of meters of their parent vent(s). Package continuity is rarely maintained over the septae between craters. Exceptions are a few packages near crater ends that contain major proportions of material ejected from vents in adjacent craters (e.g. packages F′10 and L3 in Fig. 3d,e). Where deposits are uniform and non-welded, the crater walls have clean near-vertical faces with the best cross-sectional views. On the inter-crater septae, slopes are gentler and less regular. Tack-welded veneers of juvenile material commonly adhere to these surfaces, forming one or more irregular slope-parallel layers (e.g. points marked 1 on Fig. 3c,g).

Package dispersals range from very localized, occupying only a narrow portion of a crater (e.g. package D1 in Fig. 3b), to widespread, spanning the full length of a crater and beyond (package J′2 in Fig. 3c). The more widespread packages are commonly higher in the stratigraphy (e.g. Fig. 3b,e–g). Exceptions to this rule occur in craters F and J (Fig. 3c,d), where even the basal unit 2/3 packages have large dispersals. Lateral color changes within packages are uncommon, but where they do occur (e.g. point 2 on Fig. 3g) they are gradational over tens of meters. The distinctness of bedding varies both horizontally (e.g. point 1 on Fig. 3f) and vertically (point 1 on Fig. 3e) along crater walls. Welded packages show lateral variations in their degree of welding, ranging from abrupt (e.g. point 2 on Fig. 3c) to gradational (point 2 on Fig. 3f). Welding is more common in locally dispersed packages (e.g. D5 in Fig. 3b), but strong welding does occur in a few very widespread packages (J′5 in Fig. 3c).

All craters show remarkable contrast between their northwestern and southeastern walls in characteristics such as dominant dispersal, grain size, color, and welding state. For example, in crater F, while the southeastern wall (Fig. 3d) is composed mostly of red non-welded scoria with very wide dispersal, the northwestern wall is dominated by localized packages with dark color and strong welding. The

asymmetry prevents packages from being traced or correlated across the fissure.

Dispersal variations are shown quantitatively in a plot of linear thickness half-distance measurements for 153 packages along the fissure (Fig. 4). A wide range of $t_{1/2}$ values is common in most craters. Nearly every crater contains one or more packages with $t_{1/2} \leq 20$ m (Fig. 4), similar to the equivalent $t_{1/2}$ values of recent Strombolian and Hawaiian cones (e.g. Richter et al. 1970; Heliker et al. 2003). Most craters also have more widespread packages, including a few packages with half-distances exceeding 150 m (Fig. 4). In some craters two or three separate packages are observed at equivalent stratigraphic heights (e.g. packages F′2 and F′3 on Fig. 3d), each with a distinct $t_{1/2}$ value.

## Dispersal extremes: observations at selected sections

Several craters are dominated by packages with a narrow range of dispersals. Localized packages dominate craters D and E, and widespread packages dominate craters F, H, J, and L. We expand on our general description with more detailed observations at sites that typify these dispersal extremes.

A representative section for the localized extreme is T28 on the northwestern wall of crater D (Fig. 3b), where all packages are localized, with $t_{1/2}$ between 20 and 35 m (Table 2). Many beds within the packages show various degrees of agglutination, ranging from weak tack welding to moderately strong welding where clasts adhere firmly to each other but still have distinct boundaries. Clasts of glassy, coarsely re-vesiculated rhyolite are commonly found encased in basalt. Basalt clasts generally have a red oxidized color. The grain size is coarse, and sorting is moderate to poor due to the abundance of ash-sized wall-rock particles; quantitative grain size analyses are presented in Carey et al. (in review). Basalt clast morphologies are typically ragged, slaggy, and knobbly. The wall-rock lithic content is typically 5–15% and rarely up to 40%, ranging in size from ash to 20–30-cm blocks and rare 1-m blocks.

A characteristic example of the opposite extreme is section T79 in crater F (Fig. 3d), where four of the six

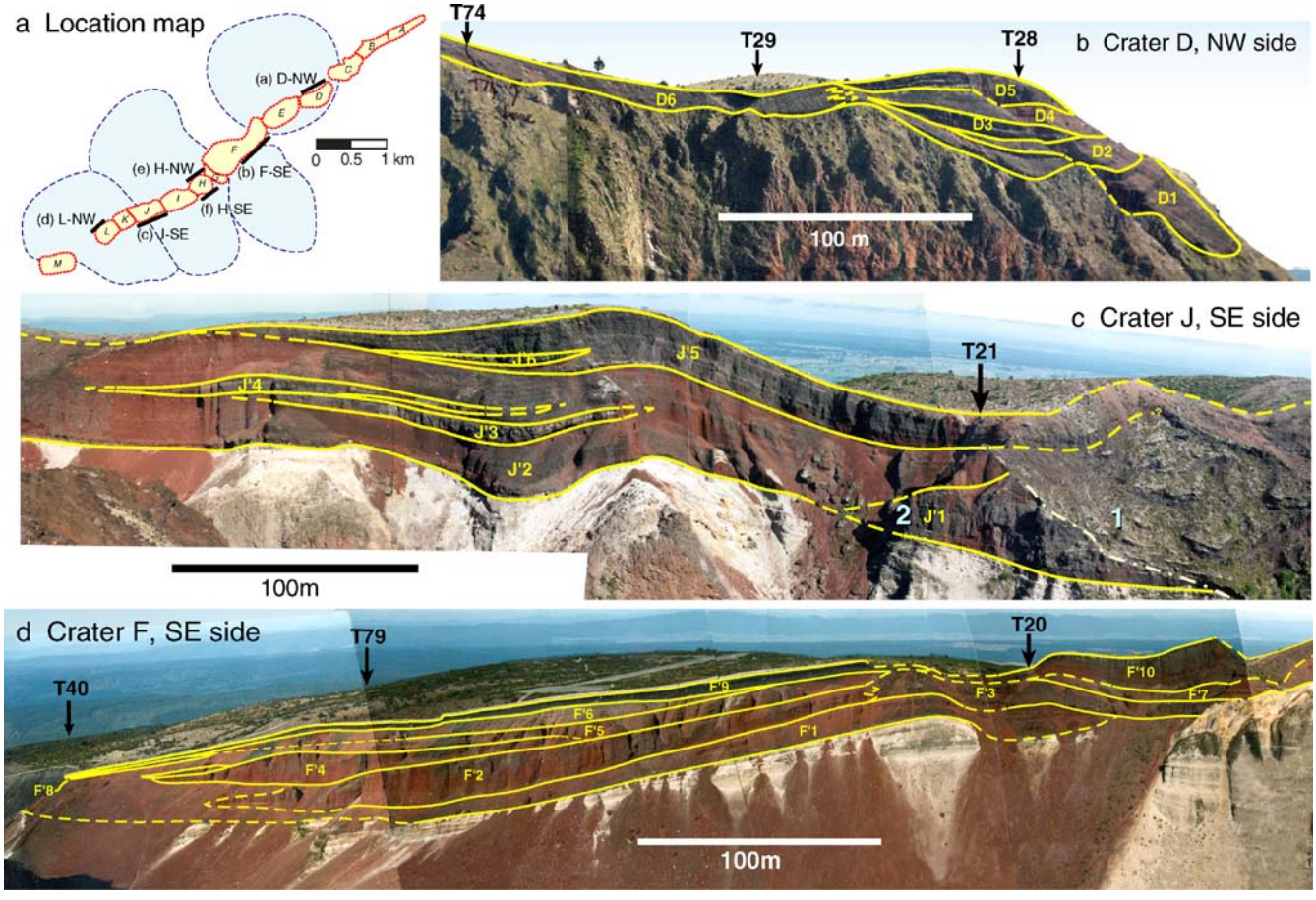


**Fig. 3** Sketches of package geometry for representative 1886 craters at Mt Tarawera. **a** Locations of lines of section; **b** northwest wall of crater D; **c** southeast wall of crater J; **d** southeast wall of crater F; **e** northwest wall of crater L; **f** northwest wall of crater H; **g** southeast wall of crater H. Locations of detailed stratigraphic sections are named and marked with *arrows*. *Numbers* refer to sites mentioned in the text. Thickness half-distance values for sections T28 and T79 are listed in Table 2

**Fig. 3** (continued)

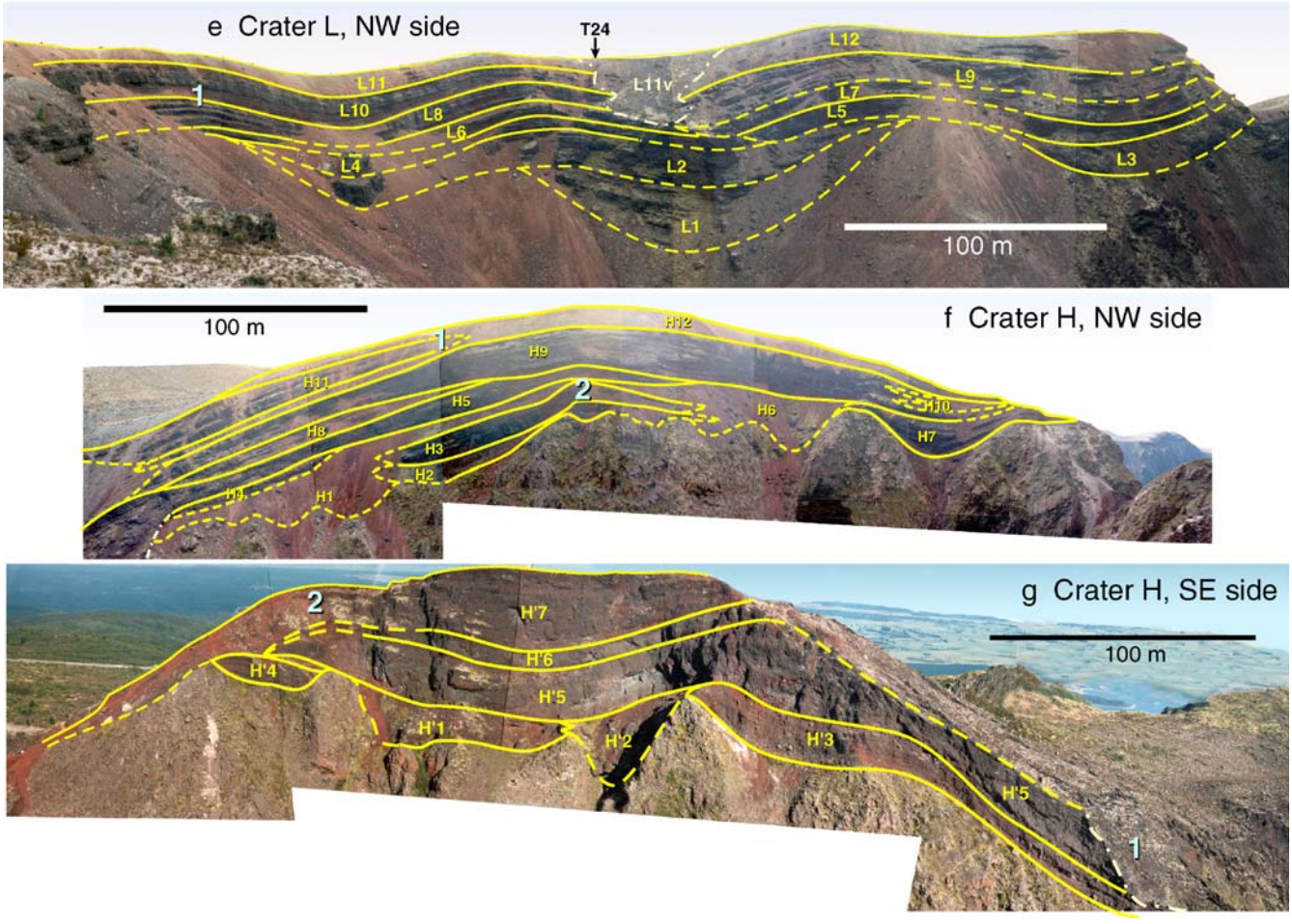


packages have $t_{1/2}$ >100 m (Table 2). Packages are typically non-welded and massive to weakly bedded. The grain size ranges from coarse ash to 10–20-cm bombs, but is dominated by fine to coarse lapilli. Wall-rock lithic content is 5–20% in the form of ash and scattered blocks. Juvenile clasts are commonly red to brown, with ragged, knobbly or blocky morphologies. Some dense cauliflower bombs are present, along with a minor proportion of slaggy clasts.

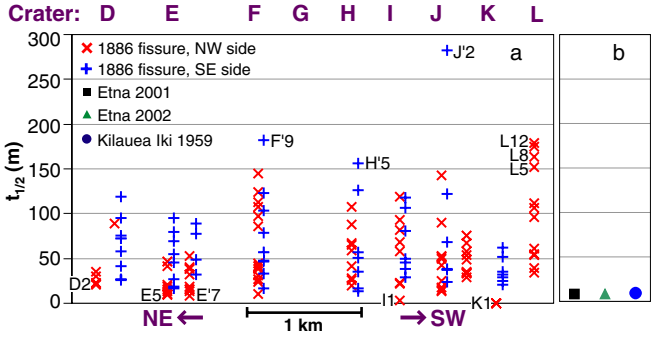


**Fig. 4** **a** Summary of linear thickness half-distance ($t_{1/2}$) values for individual packages within the 1886 proximal deposits, with different symbols for the two sides of the fissure. Crater names along the top are spaced according to the positions of their deepest portions along the fissure. Packages with extreme $t_{1/2}$ values are labeled. **b** Half-distances of three historical cones formed by Hawaiian and Strombolian explosions are shown for comparison

## Interpretations

### Accumulation rates of the 1886 deposits

Time-averaged accumulation rates during the Plinian portion of the 1886 eruption can be estimated by dividing

**Table 2** Thickness half-distance measurements for packages at stratigraphic sections T28 and T79

| Crater D, NW side | | Crater F, SE side | |
|---|---|---|---|
| Package | $t_{1/2}$, m | Package | $t_{1/2}$, m |
| | | F′9 | 123 |
| D5 | 23 | F′6 | 126 |
| D4 | 22 | F′5 | 181 |
| D3 | 30 | F′4 | 33 |
| D2 | 20 | F′2 | 103 |
| D1 | 35 | F′1 | 182 |

Sections were selected because they represent the dispersal extremes for the proximal deposits

unit 2/3 thickness values at the crater rims by an assumed duration of 5 h (Keam 1988; Houghton and Wilson 1998). The minimum thickness is 7.4 m and the maximum is 65.5 m (Fig. 2c), giving time-averaged accumulation rates ranging from 1.5 to 13 m/h.

Accumulation rates over shorter timescales can be interpreted qualitatively in greater detail from the degree of welding in the deposits (Sparks and Wright 1979). The rates varied among vents and fluctuated with time. There does not appear to be a simple relationship between accumulation rate and intensity; packages with similar degrees of welding may have $t_{1/2}$ anywhere between 5 m (e.g. package H7 in Fig. 3f) and 100 m (L10 in Fig. 3e).

The accumulation rates for several non-welded packages are above the suggested minimum rates for welding (e.g. 2–12 m/h; Sparks and Wright 1979). To explain the absence of agglutination, we consider factors that might have reduced the temperature of the ejecta before landing. The non-welded packages may contain an abundance of clasts sedimented from upper levels of the plume whose longer transport times allowed greater cooling. Greater release heights are expected to result in wider dispersals (e.g. Sparks 1986), so this idea is most compatible with the packages with large $t_{1/2}$ values. However, many non-welded packages are observed to have $t_{1/2}$ values of less than 50 m. Two alternative cooling influences could be (1) a higher content of originally cold particles of rhyolitic wall rock, or (2) some minor degree of magma-water interaction, similar to that proposed for the Tarawera Plinian phase by Walker et al. (1984) and Houghton and Wilson (1998).

## Temporal and spatial variations in eruptive behavior

The wide range in thickness half-distance values signifies a wide range of eruptive intensities in each crater. Low-intensity vents were common in all craters, but this did not preclude the presence of higher-intensity vents in close proximity. In some craters, packages with very different characteristics are laterally juxtaposed at identical stratigraphic levels. This indicates that vents less than 100 m apart were active simultaneously with contrasting eruptive styles and intensities.

The minimum time-averaged discharge rate for the 1886 eruption is $1\times10^5$ m$^3$/s ($3.9\times10^4$ m$^3$/s DRE), calculated by dividing the estimated total volume ($2\times10^9$ m$^3$; Walker et al. 1984) by the duration (5 h; Walker et al. 1984; Keam 1988). In detail, the proximal packages indicate significant variations with location and time in each of the 13 craters. The range of inferred discharge rates in single craters commonly spans at least an order of magnitude. For example, crater F (Fig. 3d) shows a high average intensity but also contains packages consistent with much less vigorous vents that may have been active only briefly. The converse is also observed, where a crater dominated by weak activity also bears evidence of an interval of intense eruption (e.g. crater E).

The temporal variations in eruptive intensity at each vent can be interpreted qualitatively, but not enough variables are constrained for more precise characterization. The changes with time in two craters at opposite dispersal extremes are illustrated schematically (Fig. 5). Vent locations are inferred to be in the deepest parts of craters and opposite the thickness maxima of the packages produced by the vents. Relative eruption intensities are interpreted from package thickness half-distances; accumulation rates are inferred from observed degrees of welding; timings are interpreted from positions in the stratigraphy; and durations are estimated from package thickness, adjusted for differences in accumulation rate.

At the earliest stage of the eruptive phase that produced proximal unit 2/3, two vents were active in crater D, one at the crater's northeast end and one slightly southwest of the crater's center (Fig. 5a). Activity at the northeastern vent was quite weak, but the accumulation rate fluctuated

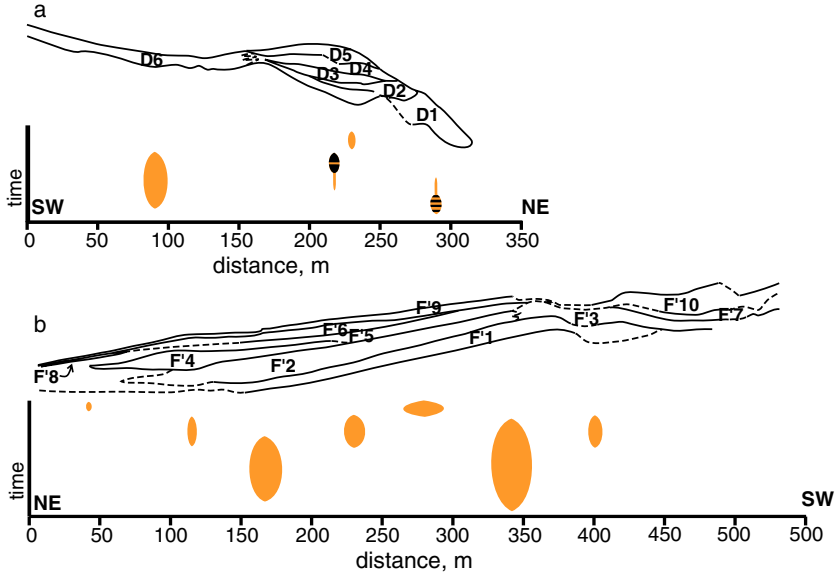


**Fig. 5** Diagrams showing changes in vent position and behavior with time for **a** northwest wall of crater D and **b** southeast wall of crater F. Width of symbol signifies intensity. *Shade* indicates accumulation rate (*black* is high, *gray* is low). Distances in meters; time axis is not quantitatively constrained. Note that there is no one-on-one correspondence between number of vents and number of packages. Source of package F′10 is believed to be located in the NE end of crater G, and is thus not shown in this diagram

**Table 3** Parameters for several cone-forming eruptions

| Eruption | $t_{1/2}$ | Final cone height (m) | Time in eruption (hours) | Average acm. rate | Max. acm. rate |
|---|---|---|---|---|---|
| Tarawera 1886 (T28)[a] | 26 m | 65 m | 5 h | 13 m/h | |
| Tarawera 1886 (T79)[a] | 171 m | 46 m | 5 h | 9 m/h | |
| Asama 1783[b] | 35 m | 70 m | 1440 h | 0.05 m/h | 3.3 m/h |
| Etna 2001[c] | 8.2 m | 62 m | 288 h | 0.2 m/h | |
| Etna 2002[d] | 8.0 m | 150 m | 816 h | 0.2 m/h | |
| Oshima 1986[e] | 33 m | 40 m | 7 h | 6 m/h | |
| Kilauea Iki 1959[f] | 9.7 m | 50 m | 864 h | 0.06 m/h | |
| Kilauea (Pu'u 'O'o) 1983–86[g] | 34 m | 255 m | 1128 h | 0.2 m/h | 2.0 m/h |
| Lonquimay (Navidad) 1988[h] | 17 m | 210 m | 240 h | 0.9 m/h | 2.1 m/h |
| Pacaya 1981[i] | 23 m | 148 m | 672 h | 0.2 m/h | 3.0 m/h |
| Paricutin 1943–44[j] | 14 m | 324 m | 1800 h | 0.2 m/h | 3.0 m/h |
| Tolbachik (cone I)1975[k] | 21 m | 330 m | 528 h | 0.6 m/h | 4.7 m/h |
| Tolbachik (cone II) 1975[l] | 12 m | 270 m | 720 h | 0.4 m/h | 2.1 m/h |
| Tolbachik (cone III) 1975[l] | 6.1 m | 140 m | 240 h | 0.6 m/h | 2.3 m/h |
| Veniaminof 1983[i] | 29 m | 150 m | 168 h | 0.9 m/h | |

The Tarawera $t_{1/2}$ data are averages over the packages at each of two stratigraphic sections. Average accumulation rates are calculated from cone height and time in eruption (quiescent intervals are not included). Maximum accumulation rates measured over shorter time intervals are indicated where available. Most of the deposits are listed by Riedel et al. (2003)

*References*:

[a]this paper, [b]Yasui and Koyaguchi (2004), [c]Calvari and Pinkerton (2004), [d]Andronico et al. (2005), [e]Sumner (1998), [f]Richter et al. (1970), [g]Heliker et al. (2003), [h]SEAN (1988), [i]McClelland et al. (1989), [j]Bullard (1947), Foshag and Gonzales (1956); [k]Fedotov et al. (1978), Tokarev (1983); [l]Fedotov et al. (1978)

greatly and at times was high enough to promote agglutination of clasts. The southwestern vent erupted with greater intensity and lower, less variable accumulation rate, so its deposit (package D6) is more widespread, less welded, and more uniform. Activity at the northeastern vent waned and then ceased midway through the main phase, but the southwestern vent was active nearly to the end of the phase. At approximately the same time that the vent at the far northeastern end of crater D expired, another vent became active just northeast of the crater's center (Fig. 5a). This central vent's maximum intensity was comparable to that of the far northeastern vent. After a brief period of consistently weak activity, the vent shifted about 10 m to the northeast and resumed activity at a slightly weaker level, then finally stopped. We infer this shift based on the observation that the upper packages on the northwestern side of crater D are offset toward the northeast. The shift may have involved the death of one vent and the birth of a new one nearby. Alternatively, the offset packages may all originate from the same vent but may have been affected by a change in ejection angle.

In crater F (Fig. 5b), vents erupted with relatively high intensity from the beginning of the phase that produced proximal unit 2/3. Material was first ejected from a vent slightly southwest of the center of this elongate crater. This vent had a high intensity and was long-lived, producing package F′1 and contributing to packages F′2, F′3, F′5, and F′9. Shortly after the first vent became active, a second one started about 150 m northeast of it (Fig. 5b). It was also intense and long-lived. Later on in this eruptive phase, a few weaker vents began to contribute some localized material, starting at roughly the same time that activity at the more intense vents was waning. The relative timing of the initiation of the weaker vents and the termination of the more intense vents is uncertain, so it is unclear whether the shifts in activity are causally related. The main phase in crater F closed with a final burst of relatively intense activity from a vent near the crater's center.

Some of the divisions between packages in proximal unit 2/3 resemble bedding planes; this raises the question of whether the Plinian eruption was discontinuous, with locally dispersed packages accumulating during pauses in activity at the more intense vents. Walker (1980) showed that pauses or periods of reduced intensity in an eruption can be marked by fine-grained beds, bedding planes, or ash partings, if the interval of decreased activity is longer than the transport time for lapilli and bombs. In the Novarupta 1912 Plinian deposits, Houghton et al. (2004b) observed bedding planes within but not beyond 10 km from vent. They calculated the maximum time for 5 cm pumices to travel that far, and concluded that the eruption never paused longer than 15 min.

We apply the same chain of reasoning to the Tarawera 1886 deposits. Ash partings are absent and lapilli with ≥2 cm diameter are present in every level of the deposits within 12 km from vent. The average density of Tarawera juvenile clasts is ~1,000 kg $m^{-3}$ (Carey et al. in review). The time to rise to the top of a 28 km plume is ~250 s (Walker et al. 1984; Hort and Gardner 2000). The time for particles to travel 12 km laterally within the umbrella cloud

is estimated to be 200 s, based on umbrella cloud models (Sparks 1986; Bonadonna and Phillips 2003) and observed propagation speed of the Mt St Helens ash plume front (Sarna-Wojcicki et al. 1981). The fall time from the umbrella cloud is 750 s (Wilson 1972). This sums to a total travel time of 20 min for a 2-cm lapillus. We conclude that during the main (unit 2/3) phase of the eruption, the Plinian plume never stopped for longer than ~20 min, although individual vents may have started and stopped activity at different times within that duration.

The cessation of intense activity cannot be precisely correlated among craters due to local variations in accumulation rate. Magma withdrawal accompanying the transition to the weaker final phreatomagmatic (unit 4/5) phase was associated with vent wall collapse. The outward dip of beds along most of the fissure is a result of late-stage faulting and slumping during and after the deposition of phreatomagmatic unit 4/5, such that nearly all the inward-dipping inner-wall beds are gone. In some areas, collapse was relatively gradual and progressive, resulting in angle-of-rest slopes. At other locations, the walls remained stable throughout the main phase, but when the magma retreated, large segments of the walls failed, leaving near-vertical surfaces. The slope-parallel tack-welded veneers of juvenile material covering several slopes were probably generated in the closing stage of the eruption. Ejecta from weak explosions adhered best to the scarp surfaces with the gentlest slopes.

## Asymmetry across the fissure

The asymmetry in deposit characteristics across the fissure may be partially explained by the influence of wind on the plume. For the first half of the eruption, the wind blew toward the north, across the fissure. We envision that, at this time, the peak of downwind accumulation of material from the upper convective region of the Plinian plumes was displaced outward, beyond the very proximal area. In contrast, clasts released from lower heights were less affected by wind and concentrated immediately downwind from source in a manner described for the Pu‘u ‘O‘o and Kilauea Iki eruptions (Richter et al. 1970; Heliker et al. 2003). In craters that hosted intense activity starting early in the eruption, this combination of wind effects would result in packages of more limited apparent dispersal on the downwind (northwestern) side of the fissure. Observations in craters F, H, and J are consistent with this idea (Figs. 3 and 4). Another source of the cross-fissure asymmetry, considered in the discussion, is uneven sedimentation associated with heterogeneities in the jet portion of the plume.

## Locations of Plinian vents

Our detailed study of package dispersals has illuminated patterns of eruptive intensity in several craters. Most craters are dominated by low-intensity vents. Sporadic high-intensity activity occurred in several parts of the fissure, but truly sustained intense activity was restricted to only a few locations. Four craters are dominated by widespread packages: F, H, J, and L (Fig. 3c–f). Vents within these craters are the most likely locations for the high-intensity sources that fed the Plinian umbrella cloud.

The four intense sources did not necessarily start and stop at the same time. Widespread packages typically occur in the middle to upper levels of the unit 2/3 stratigraphy, suggesting that eruption intensity increased with time over most of the fissure. However, craters F and J have widespread packages at the base of unit 2/3, and we interpret that high-intensity vents in these craters began erupting very early in the eruption and maintained their high intensities through the full duration of the main (unit 2/3) phase. Thus it seems that the early high column was mostly fed from vents in craters F and J.

## Comparison with cone-forming deposits

To develop an appropriate model for the dynamics of the 1886 eruption, we examine current plume models and consider our package dispersals and accumulation rates in a global context. Table 3 presents published heights, durations, and accumulation rates for some historical cone-forming eruptions that lacked Plinian phases. The eruptions include Strombolian (e.g. Pacaya 1981: McClelland et al. 1989), Hawaiian (e.g. Kilauea Iki 1959: Richter et al. 1970), “violent Strombolian” (e.g. Paricutin: Cashman et al. 2004), and sub-Plinian (e.g. Asama 1783: Yasui and Koyaguchi 2004) examples. Average accumulation rates were calculated from cone height and total eruption duration, and maximum accumulation rates for shorter intervals were recorded by observers during some of the eruptions. The average accumulation rates for most of these eruptions are an order of magnitude lower than the 9–13 m/h calculated for the selected Tarawera 1886 sites. Even the maximum accumulation rates of the other examples are typically only 1–3 m/h. The relatively high rate of 6 m/h for Oshima 1986 was associated with unusually vigorous Hawaiian-style fountaining (Sumner 1998).

We have calculated approximate linear thickness half-distances from the dimensions of the cones in Table 3. Each cone’s $t_{1/2}$ represents an average dispersal over the whole cone-forming eruption (individual beds cannot be identified). The $t_{1/2}$ values for the Hawaiian–Strombolian cones range between 6 and 30 m. Of the 154 Tarawera packages that were measured, 45 have $t_{1/2}$ values in this range, including the five at section T28 (Table 2). This confirms that some packages are dominated by clasts from weak explosions analogous to the historical cone-building eruptions. The maximum heights reached by these clasts could have ranged between 250 and 700 m, by comparison with measurements of historical lava fountaining eruptions (Table 4). However, many Tarawera packages have significantly wider dispersals: 50% of packages have $t_{1/2}$

**Table 4** Average and maximum fountain heights for four Hawaiian eruptions and one sub-Plinian eruption (Oshima) that featured Hawaiian-style fountaining

| Eruption | Average fountain height | Max. height |
|---|---|---|
| Etna 2001[a] | 250 m | 250 m |
| Etna 2002[b] | 270 m | 500 m |
| Kilauea Iki 1959[c] | 230 m | 670 m |
| Pu'u 'O'o 1983–86[d] | 270 m | 470 m |
| Oshima 1986[e] | 500 m | 1600 m |

*References*:
[a]INGV (2001), [b]INGV (2002), [c]Richter et al. (1970), [d]Heliker et al. (2003), [e]Sumner (1998)

values over 50 m, and 18% have $t_{1/2}$ >100 m, with a maximum of 283 m (crater J; Fig. 3c, Fig. 4).

To determine the exact style of activity at Tarawera's weakest vents, we revisit section T28, because the site is overwhelmingly dominated by localized packages (average $t_{1/2}$=26 m; Table 2). The clasts in the T28 packages are red, oxidized, ragged, and blocky. Clasts do not have highly fluidal shapes or glassy rinds as would be expected in products of Hawaiian fountains (Heiken and Wohletz 1985). Lithic content at T28 ranges averages 17% (Carey et al. in review), much higher than typical for Hawaiian lava fountains (e.g. less than 1% for Kilauea Iki 1959; B. Houghton unpublished data). The deposits are bedded, suggesting intermittent explosions. We thus conclude that the style of the weak vents was Strombolian.

## Comparison with Plinian deposits

Suitable comparisons between the Tarawera 1886 deposit and other Plinian deposits are limited, because very few Plinian deposits exist with exposures so close to vent. One Plinian deposit where proximal products are preserved is from the andesite-dacite eruption of Novarupta 1912 (Fierstein and Hildreth 1992; Fierstein et al. 1997; Houghton et al. 2004b). The very proximal (<1 km from vent) ejecta ring at Novarupta grew within a ~24-hour interval (Fierstein et al. 1997). The ejecta ring's thickness ranges up to 250 m, giving average accumulation rates up to 10 m/h. This value fits within the range of accumulation rates calculated for Tarawera, suggesting that the plumes in these two eruptions may have behaved similarly. The model that we will propose includes some features from that of Fierstein et al. (1997), adapted to a basaltic system for Tarawera 1886.

The dispersals of the Tarawera 1886 deposit and other Plinian deposits are compared on a plot of log thickness vs. square root of area (Fig. 6; Pyle 1989). The extent of the Tarawera 1886 deposit appears limited compared to the other Plinian deposits only because much of the 1886 fall landed in the ocean (Walker et al. 1984). The 1886 proximal and medial-distal deposits have thickness half-distances ($b_t$ calculated from isopach areas after Pyle 1989) of 0.05 km and 4.3 km, respectively, showing that the proximal deposits have a much greater rate of thinning. The best-fit exponential curves intersect at 0.53 km on the square root of area axis (Fig. 6), equivalent to a distance of 300 m from vent. This is approximately consistent with field observations of a change from steeper to gentler slopes 300–400 m out from the edges of the Mt Tarawera rift.

Many Plinian deposits have two or more exponential thinning trends that appear as line segments with different slopes on the log thickness-area$^{1/2}$ plot (Pyle 1989; Fierstein and Hildreth 1992; Hildreth and Drake 1992; Sparks et al. 1992). Bonadonna et al. (1998) proposed a model to explain the multiple segments. The innermost and steepest segment signifies fallout from the margins of the convective region of the plume (Ernst et al. 1996). The junction between this segment and the next represents the "corner", where the sedimentation mechanism changes from shedding from the plume margins to vertical fallout from the umbrella cloud, with possible advection

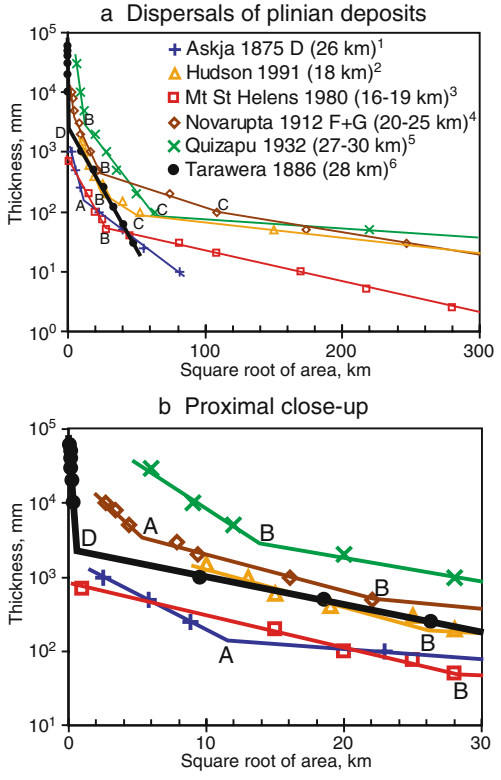


**Fig. 6** Plots of ln thickness vs. square root of area (after Pyle 1989) comparing Tarawera 1886 with other Plinian deposits. Breaks in slope are lettered according to their interpreted sedimentation regimes (after Bonadonna et al. 1998), as follows: **A** transition from plume margin to large Reynolds number umbrella cloud sedimentation; **B** transition from large to intermediate/mixed Reynolds number sedimentation from the umbrella cloud; and **C** transition from intermediate/mixed to small Reynolds number sedimentation from the umbrella cloud. Point *D*, at an equivalent radius of 300 m, is much closer to vent than the points labeled *A*. Large-scale view for context, with observed or calculated column heights in parentheses (**a**). Close-up highlights the contrasting positions of the breaks in slope (**b**). References: *1* Sparks et al. (1981); *2* Scasso et al. (1994), Bonadonna et al. (1998); *3* Carey and Sigurdsson (1982), Carey and Sparks (1986); *4* Fierstein and Hildreth (1992); *5* Hildreth and Drake (1992); *6* Walker et al. (1984), this paper

by wind (e.g. Sparks et al. 1997; Bonadonna and Phillips 2003). More distal line segments represent other umbrella cloud regimes where sedimentation is dominated by different particle Reynolds numbers (Bonadonna et al. 1998). Not all segments are observed for all deposits due to differences in preservation and methods of data collection.

The most proximal line segments of the Novarupta units F and G and Askja unit D deposits probably indicate column margin sedimentation (Bursik et al. 1992; Ernst et al. 1996), because the breaks in slope (labeled A on Fig. 6) fall within the estimated distances to the plume corners based on the columns' respective heights (Bonadonna et al. 1998). However, the innermost segments for the Quizapu, Hudson, and Mount St Helens deposits are too far from vent to be related to the plume margins, and instead probably represent the large Reynolds number regime of sedimentation from the umbrella cloud (Bonadonna et al. 1998). The most proximal part of the Tarawera 1886 deposit is unique among these deposits: the line segment is much steeper, and the break in slope is positioned much closer to vent, than in the other trends on Fig. 6. This is interpreted to be due to sedimentation from much lower heights than postulated for any of the other eruption plumes.

## Discussion

In preparation for developing a sedimentation model for Tarawera 1886, we summarize the important aspects of the proximal deposits that must be considered: (1) the majority of the proximal packages have $t_{1/2}$ values greater than typical values for Hawaiian–Strombolian deposits (Fig. 4); (2) proximal thicknesses of up to 70 m (Fig. 2) indicate near-vent accumulation rates that greatly exceed those recorded for Hawaiian and Strombolian explosions; (3) the overall proximal deposit has, however, an extremely rapid rate of thinning and is confined to within 400 m of vent, compared to 3 km or more for deposits inferred to have sedimented from the margins of the convective portions of other Plinian plumes (Fig. 6); (4) the proximal deposits contain a considerable proportion of fine particles.

### Plume models

A simple plume sedimentation model assumes that all non-ballistic particles are swept up to the full height of the plume and are released from the base of the umbrella cloud (Sparks et al. 1997). Sedimentation starts at the eruption column's "corner," the point where the ascending convective plume reaches neutral buoyancy and the gas/clast suspension begins to spread laterally. Only ballistic particles are deposited within the zone between vent and corner, typically 1–10 km from vent (Sparks et al. 1997 and references therein; Bonadonna and Phillips 2003). A simple model thus does not account for the overthickened and yet relatively fine-grained proximal deposits observed at Tarawera.

Recent plume models (Bursik et al. 1992; Ernst et al. 1996) add a second transport regime consisting of the turbulent margins of the convective region of the plume. Particles may be released or re-entrained by eddies depending on grain size and height within the column. To make the equations workable, these models generally average the velocity across the plume, effectively assuming a "top hat" or uniform velocity profile. The turbulent eddies are added along the boundary between the ascending plume and the still atmosphere. For a 25 km plume, pumices <1 m are totally re-entrained at heights up to 5 km within the plume, and pumices <1 cm are totally re-entrained to the full height of the plume (Ernst et al. 1996). This implies that no particles smaller than 1 cm can accumulate inside the position of the plume corner, estimated to be ~6 km from vent for the 25 km column example (Bonadonna and Phillips 2003). No particles <1 m can accumulate within about 2 km of vent (Sparks 1986). In these models, re-entrainment becomes especially important for smaller particles and more intense plumes, resulting in reduced accumulation rate within a few hundred meters of vent (Bursik et al. 1992, Ernst et al. 1996). These models' predictions are not consistent with the overthickened and yet relatively fine-grained proximal deposits observed at Tarawera.

Riedel et al. (2003) adapted these models for eruptions with coarse grain size distributions and low eruption velocities such as Hawaiian-style fountains. Their "jet fallout" version of the model and an alternative model of ballistic transport with drag provided equally good fits to data for rapidly accumulated cone-forming deposits. The authors suggested that proximal overthickening in Plinian deposits could form by fallout of coarse particles from the margins of the jet region of the column. Our proximal deposits are, however, too fine-grained (Table 1) to fit such a model of jet margin sedimentation. Another problem is that no single model can explain the very large range of dispersals at Tarawera.

### Significance of Tarawera's intermediate thickness half-distances

The $t_{1/2}$ values of deposits from typical Plinian umbrella clouds range from ~4 km to >100 km (calculated from $b_t$ based on isopachs; Pyle 1989). At the other extreme, most Hawaiian–Strombolian deposits have $t_{1/2} \leq 20$ m (e.g. Richter et al. 1970; Calvari and Pinkerton 2004; Andronico et al. 2005). Most of the values for Tarawera 1886 fall between these two characteristic ranges (Fig. 4).

One possible cause for the intermediate $t_{1/2}$ values is mixing of material from the top of the convective region of one or more of the 1886 plumes ($t_{1/2} \approx 4$ km) with material from nearby Strombolian explosions ($t_{1/2} \approx 20$ m). We tested this idea by modeling the apparent $t_{1/2}$ value arrived at by adding a widespread layer with a maximum thickness ($T_0$) value of 3 m and a $t_{1/2}$ value of 4 km to a wedge with a $T_0$ of

84 m and a $t_{1/2}$ value of 28 m (the thickness and average $t_{1/2}$ for unit 2/3 at section T28). The $t_{1/2}$ value of the combination is 31 m. For the $t_{1/2}$ to increase above 100 m, the widespread fall component would need to be much thicker, with $T_0$=80 m. Thus the intermediate (100–280 m) $t_{1/2}$ values are not adequately explained by mixing of clasts from the umbrella cloud with products of low-intensity vents.

We infer that the Tarawera 1886 proximal segment must reflect sedimentation from levels lower than the typical release heights in the other Plinian plumes, yet higher than the typical maximum heights attained by lava fountains and Strombolian explosions. A large amount of material with a wide grain size range accumulated very close to vent at a rapid rate, up to an order of magnitude higher than accumulation rates recorded for typical Hawaiian–Strombolian eruptions (Table 3). We suggest that the Tarawera 1886 eruption featured substantial sedimentation from the margins of low portions of the column, including the lower convective region and especially the momentum-driven jet region that makes up the basal 1–4 km (Sparks 1986). This requires that the jet margin regime be a very important contributor of clasts of all grain sizes, in contrast to what is depicted in current jet-margin sedimentation models (e.g. Ernst et al. 1996; Riedel et al. 2003).

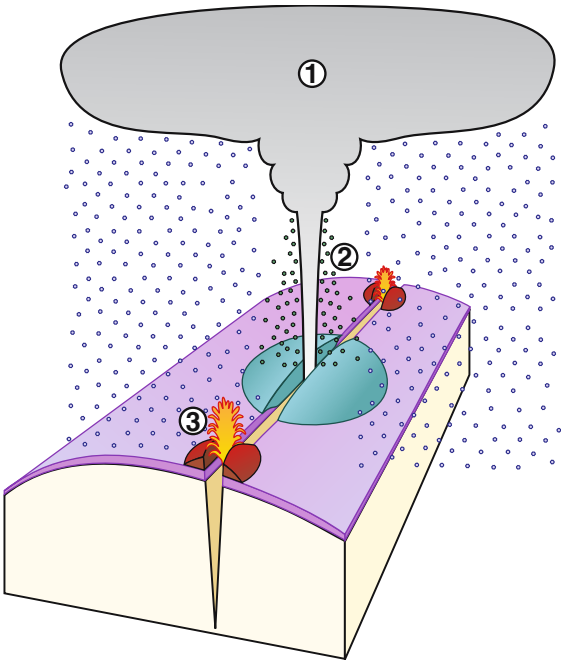


**Fig. 7** Cartoon with schematic depictions of three transport regimes. Upper plume (*1*): particles are carried to the full height of the plume, travel laterally due to wind or buoyancy controlled spreading, and are showered predictably over both proximal and distal areas. Margins of jet and lower convective plume (*2*): the relatively low velocity, unsteady motion and high particle concentration along the margins allow particles of all sizes to escape and land in the proximal area. Low-intensity Strombolian explosions (*3*)

## Model and implications

Our proximal sedimentation model for the Tarawera 1886 eruption is heavily based on a recent model for the Novarupta 1912 eruption (Houghton et al. 2004b). The Novarupta deposits include beds with $t_{1/2}$ values of between 20 and 400 m located within 3 km of vent, defining a cone of fall ejecta (the "ejecta ring") and surrounding sector-confined wedges of fall lapilli (Fierstein et al. 1997; Houghton et al. 2004b). Fall units 1 and 2 at Novarupta (Houghton et al. 2004b) are the only deposits we know of worldwide with complex proximal structure and $t_{1/2}$ values comparable to those at Tarawera. The data of Fierstein et al. (1997) and Houghton et al. (2004b) show that the sedimentation that built Novarupta's ejecta ring was both episodic and confined to narrow sectors. To achieve a sufficiently high rate of deposition to account for the full proximal deposit thickness, they suggested that the jet had a Gaussian velocity profile, allowing more material to be released from the slower-moving margins. They also suggested that the non-systematic variation in sedimentation of the 1912 deposits was due to unsteadiness and heterogeneity in the pulses of material entering the jet region of the 1912 plumes.

We propose that deposition in the proximal environment during the Tarawera 1886 eruption included three elements (Fig. 7): (1) clasts released from near the full height of the Plinian plumes, i.e. upper margins of the convective region (Sparks et al. 1997); (2) particles shed from the margins of the jet and possibly lower convective regions of the plumes; and (3) ejecta from Strombolian vents that did not contribute significantly to the Plinian plumes. The eruption featured at least two (craters F and J), and probably up to four (craters H and L) principal sources for the Plinian columns, along with Strombolian-style explosions from dozens of other vents along the fissure. At least one of the high-intensity vents and many of the weaker vents were active at any given time during the phase that produced proximal unit 2/3. The idea of multiple vents feeding a single shared umbrella cloud (Walker et al. 1984) is consistent with some eyewitness accounts that describe between three and seven discrete columns (Keam 1988).

To explain the contribution of the jet portions of the Plinian plumes, we require a modified model for transport dynamics that includes a more realistic velocity profile in the jet, permitting substantial sedimentation from the jet margins. Classical fluid dynamical theory predicts that the magma in the upper conduit ascends more slowly along the margins (e.g. Holman 1992; Dobran 2001). We suggest that the jet perpetuates a curved velocity profile inherited from the mixture ascending in the upper conduit. We also suggest that jet margin sedimentation is highly variable due to asymmetries and fluctuations in particle concentration in the mixture entering the jet.

Although the multiple-vent configuration at Tarawera is rare, our conceptual model for complex proximal sedimentation may apply to many Plinian eruptions. In particular, it may be common for a Plinian column to release particles both from near its full height and from the margins of the jet and lower convective plume. Descriptions of two recent sub-Plinian eruptions (Asama 1783 and

Oshima 1986) suggest that they were also characterized by sedimentation from both the high plume and from lower elevations on the margin of the plume, implying that such mingling may be more common than previously thought (e.g. Sumner 1998; Yasui and Koyaguchi 2004). Unfortunately, the data from these sub-Plinian eruptions lack sufficient detail for quantitative comparison with the 1886 proximal deposits.

We suggest that sedimentation models sacrifice accuracy by assigning a uniform average velocity across the jet, and that the Gaussian velocity profile across the jet needs to be emphasized (e.g. Carey and Sparks 1986; Sparks et al. 1997). Lower velocities along the jet margins allow near-vent deposition of a larger volume of material with a significant proportion of fine particles. While models tend to assume steady-state conditions to facilitate calculations, our data indicate that the jet regions of Plinian plumes are likely to be highly variable and heterogeneous.

## Conclusions

The unusually high quality of preservation and exposure close to the Tarawera 1886 vents has facilitated a detailed study of proximal deposition of a Plinian eruption. The 1886 Tarawera proximal deposits have a complex geometry reflecting deposition from several regions within Plinian plumes, together with coeval Strombolian-style eruption from other vents. We observe a wide range in the thicknesses and geometry of proximal deposit packages, reflecting strongly varying intensities for the vents along the fissure. The $t_{1/2}$ values of most packages are intermediate between typical basaltic (Hawaiian-Strombolian) and typical Plinian dispersals, suggesting that every package is a mixture of a widely dispersed component that fell from the upper margins of the Plinian plume and a locally dispersed component that is a combination of (1) ejecta from weakly explosive vents that did not contribute to the high plume and (2) particles from the margins of the jet and lower convective plume. Though the Strombolian vents may not have contributed much material to the high plume, the air heated above them could have contributed substantially to the buoyancy of the high plume and enhanced its vigor (e.g. Houghton et al. 2004b and references therein).

The vents that contributed most to the high plume were localized, not spread evenly along the fissure. Of the thirteen major craters, four (F, H, J, L) are dominated by the most widespread packages and are inferred to have contained Plinian vents, whereas other craters contributed virtually nothing to the high plume (e.g. D, E), based on their lack of widespread packages. One important conclusion is that a significant volume of particles with a wide grain size range was released from the transport regime associated with the slower-moving margins of the momentum-driven jet (lowermost 1–4 km) and the lower convective regions of the plume. The particle concentration in the jet was probably variable and asymmetric, contributing to the heterogeneity in the proximal deposits.

The proximal deposits of Tarawera 1886 are unusual, but they may not be unique. Overthickened proximal deposits are probably produced in most Plinian eruptions but rarely preserved. Caldera collapse, pyroclastic density currents, secondary remobilization processes, and lava dome growth may remove or obscure the proximal deposits of Plinian eruptions at other volcanoes.

**Acknowledgements** This research was supported by NSF grant EAR01-25719. We thank Michael Rosenberg of IGNS, Wairakei, for invaluable assistance in the field and lab. CJNW thanks the UK NERC and the New Zealand Foundation for Research, Science & Technology for financial support. The manuscript benefited greatly from the constructive comments of Costanza Bonadonna, Takehiro Koyaguchi, Steve Self, and James White. We also thank Gary Barnes, Julia Hammer, Andrew Harris, and Don Swanson for thorough and helpful comments on the draft manuscript.

## References

Andronico D, Branca S, Calvari S, Burton M, Caltabiano T, Corsaro R, Del Carlo P, Garfi G, Lodato L, Miraglia L, Mure F, Neri M, Pecora E, Pompilio M, Salerno G, Spampinato L (2005) A multi-disciplinary study of the 2002–03 Etna eruption: insights for a complex plumbing system. Bull Volcanol 67(4):314–330

Bonadonna C, Phillips J (2003) Sedimentation from strong volcanic plumes. J Geophys Res 108:2340–2368

Bonadonna C, Ernst GGJ, Sparks RSJ (1998) Thickness variations and volume estimates of tephra fall deposits: the importance of particle Reynolds number. J Volcanol Geotherm Res 81(3–4): 173–187

Bullard FM (1947) Studies on Paricutin Volcano, Michoacan, Mexico. Geol Soc Am Bull 58:433–450

Bursik MI, Sparks RSJ, Gilbert JS, Carey SN (1992) Sedimentation of Tephra by volcanic plumes. 1. Theory and its comparison with a study of the Fogo-a Plinian Deposit, Sao-Miguel (Azores). Bull Volcanol 54(4):329–344

Calvari S, Pinkerton H (2004) Birth, growth and morphologic evolution of the 'Laghetto' cinder cone during the 2001 Etna eruption. J Volcanol Geotherm Res 132:225–239

Carey R (2002) A volcanological study of the proximal deposits from the 1886 Tarawera eruption. MSc Thesis, School of Earth Sciences, University of Tasmania, Hobart, Australia, p 103

Carey SN, Sigurdsson H (1982) Influence of particle aggregation on deposition of distal tephra from the May 18, 1980 eruption of Mount St. Helens volcano. J Geophys Res 87:7061–7072

Carey S, Sparks RSJ (1986) Quantitative models of fallout and dispersal of tephra from volcanic eruption columns. Bull Volcanol 48:109–125

Cashman K, Delgado H, Johnson E, Pioli L, Rosi M, Wallace P (2004) A new look at violent Strombolian eruptions: past behavior and future potential. Abstracts, IAVCEI General Assembly 2004, Pucon, Chile

Cole JW (1970) Structure and eruptive history of the Tarawera Volcanic Complex. NZ J Geol Geophys 13:879–902

Dobran F (2001) Volcanic processes: mechanisms in material transport. Kluwer, New York, p 590

Ernst GGJ, Sparks RSJ, Carey SN, Bursik MI (1996) Sedimentation from turbulent jets and plumes. J Geophys Res 101:5575–5589

Fedotov SA, Enman VB, Magus'kin MA, Levin VY, Zharinov NA (1978) Intrusion of basalts and the formation of feeder fissures for the great 1975 Tolbachik eruption, as inferred from geodetic data. Akademii Nauk Doklady Earth Sci Sect 229:43–46

Fierstein J, Hildreth W (1992) The plinian eruptions of 1912 at Novarupta, Katmai National Park, Alaska. Bull Volcanol 54: 646–684

Fierstein J, Houghton BF, Wilson CJN, Hildreth W (1997) Complexities of plinian fall deposition at vent: an example from the 1912 Novarupta eruption (Alaska). J Volcanol Geotherm Res 76:215–227
Foshag W, Gonzales R (1956) Birth and development of Paricutin volcano. U S Geol Surv Bull 965(D):355–489
Heiken G, Wohletz K (1985) Volcanic Ash. University of California Press, Berkley, p 246
Heliker CC, Kauahikaua J, Sherrod DR, Lisowski M, Cervelli PF (2003) The Rise and fall of Pu'u 'O'o Cone, 1983–2002. US Geol Surv Prof Paper No. 1676, USGS, Reston, VA, pp 29–51
Hildreth W, Drake RE (1992) Volcano Quizapu, Chilean Andes. Bull Volcanol 54:93–125
Holman J (1992) Heat transfer. McGraw-Hill, London, pp 713
Hort M, Gardner J (2000) Constraints on cooling and degassing of pumice during Plinian volcanic eruptions based on model calculations. J Geophys Res 105:25981–26001
Houghton BF, Wilson CJN (1998) Fire and water: physical roles of water in large eruptions at Taupo and Okataina calderas. In: Arehart GB, Hulston JR (eds) Water-rock interaction. Proceedings of the 9th International Symposium on Water-Rock Interaction, 30 March–3 April 1998, Taupo, New Zealand, AA Balkema, Rotterdam, pp 25–30
Houghton BF, Wilson CJN, Del Carlo P, Coltelli M, Sable JE, Carey RJ (2004a) The influence of conduit processes on changes in style of basaltic Plinian eruptions: Tarawera 1886 and Etna 122 BC. J Volcanol Geotherm Res 137:1–14
Houghton BF, Wilson CJN, Fierstein J, Hildreth W (2004b) Complex proximal deposition during the Plinian eruptions of 1912 at Novarupta, Alaska. Bull Volcanol 66:95–133
Hutton FW (1887) The eruption of Mount Tarawera. J Geol Soc Lond 43:178–189
Istituto Nazionale di Geofisica e Vulcanologia (INGV) (2001) Unita Funzionale Vulcanologia e Geochimica Report. Retrieved October 2005 from http://www.ct.ingv.it/Ufvg/Default.htm
Istituto Nazionale di Geofisica e Vulcanologia (INGV) (2002) Unita Funzionale Vulcanologia e Geochimica Report. Retrieved October 2005 from http://www.ct.ingv.it/Ufvg/Default.htm
Keam RF (1988) Tarawera: the volcanic eruption of 10 June 1886. Published by the author, Auckland, New Zealand, pp 472
Koyaguchi T (1994) Grain-size variation of tephra derived from volcanic umbrella clouds. Bull Volcanol 56:1–9
McClelland L, Simkin T, Sumners M, Nielsen E, Stein TC (eds) (1989) Global volcanism 1975–1985. Prentice-Hall and American Geophysical Union, AGU, Washington, DC, p 653
Nairn IA (1979) Rotomahana-Waimangu eruption, 1886: base surge and basalt magma. J Geol Geophys 22(3):363–378
Nairn IA, Cole JW (1981) Basalt dikes in the 1886 Tarawera Rift. NZ J Geol Geophys 24(5–6):585–592
Pyle DM (1989) The thickness, volume and grain-size of tephra fall deposits. Bull Volcanol 51:1–15
Richter DH, Eaton JP, Murata KJ, Ault WU, Krivoy HL (1970) Chronological narrative of the 1959–60 eruption of Kilauea volcano, Hawaii. U S Geol Surv Prof Paper No. 537-E, USGS, Reston, VA, p 73
Riedel C, Ernst GGJ, Riley M (2003) Controls on the growth and geometry of pyroclastic constructs. J Volcanol Geotherm Res 127:121–152
Sarna-Wojcicki AM, Shipley S, Waitt RB Jr, Dzurisin D, Wood SH (1981) Areal distribution, thickness, mass, volume, and grain size of air-fall ash from six major eruptions of 1980. In: Lipman PW, Mullineaux DR (eds) The 1980 eruptions of Mount St Helens, Washington. U S Geol Surv Prof Paper No. 1250, Reston, VA, pp 577–600
Scasso RA, Corbella H, Tiberi P (1994) Sedimentological analysis of the tephra from the 12–15 August 1991 eruption of Hudson volcano. Bull Volcanol 56:121–132
Scientific Event Alert Network (SEAN) (1988) Lonquimay (Chile) volcanic activity report. SEAN Volcanic Activity Reports 1988
Smith SP (1886a) The eruption of Tarawera: a report to the Surveyor General. NZ Government Printer, Wellington, New Zealand, pp 84
Smith SP (1886b) Preliminary report on the volcanic eruption at Tarawera. J House Represent 26:1–4
Sparks RSJ (1986) The dimensions and dynamics of volcanic eruption columns. Bull Volcanol 48:3–15
Sparks RSJ, Wright JV (1979) Welded air-fall tuffs. Geol Soc Am Spec Pap 180:155–166
Sparks RSJ, Wilson L, Sigurdsson H (1981) The pyroclastic deposits of the 1875 eruption of Askja, Iceland. Phil Trans R Soc London 229:241–273
Sparks RSJ, Bursik MI, Ablay GJ, Thomas RME, Carey SN (1992) Sedimentation of tephra by volcanic plumes. 2. Controls on thickness and grain-size variations of tephra fall deposits. Bull Volcanol 54:685–695
Sparks RSJ, Bursik MI, Carey SN, Gilbert JS, Glaze LS, Sigurdsson H, Woods AW (1997) Volcanic plumes. Wiley, Chichester, pp 574
Sumner JM (1998) Formation of clastogenic lava flows during fissure eruption and scoria cone collapse: the 1986 eruption of Izu-Oshima volcano, eastern Japan. Bull Volcanol 60:195–212
Thomas APW (1888) Report on the eruption of Tarawera and Rotomahana, NZ Government Printer, Wellington, New Zealand, pp 74
Tokarev P (1983) Calculation of the magma discharge, growth in the height of the cone and dimensions of the feeder channel of crater 1 in the Great Tolbachik fissure eruption, July 1975. In: Fedotov S, Markhinin Y (eds) The Great Tolbachik fissure eruption. Cambridge University Press, Cambridge, pp 27–35
Walker GPL (1980) The Taupo Pumice: product of the most powerful known (ultraplinian) eruption? J Volcanol Geotherm Res 8:69–94
Walker GPL, Self S, Wilson L (1984) Tarawera 1886, New Zealand: a basaltic plinian fissure eruption. J Volcanol Geotherm Res 21:61–78
Williams WL (1887) Phenomena connected with the Tarawera eruption of 10th of June as observed at Gisborne. Trans NZ Inst 19:380–382
Wilson L (1972) Explosive volcanic eruptions. II. The atmospheric trajectories of pyroclasts. Geophys J R Astron Soc 30:381–392
Yasui M, Koyaguchi T (2004) Sequence and eruptive style of the 1783 eruption of Asama Volcano, central Japan: a case study of an andesitic explosive eruption generating fountain-fed lava flow, pumice fall, scoria flow and forming a cone. Bull Volcanol 66:243–262